Direct calculation of coupled diabatic potential-energy surfaces for ammonia and mapping of a four-dimensional conical intersection seam

Shikha Nangia[a] and Donald G. Truhlar
Department of Chemistry and Supercomputing Institute, University of Minnesota, Minneapolis, Minnesota 55455-0431

(Received 8 November 2005; accepted 4 January 2006; published online 27 March 2006)

We used multiconfiguration quasidegenerate perturbation theory and the fourfold-way direct diabatization scheme to calculate *ab initio* potential-energy surfaces at 3600 nuclear geometries of NH_3. The calculations yield the adiabatic and diabatic potential-energy surfaces for the ground and first electronically excited singlet states and also the diabatic coupling surfaces. The diabatic surfaces and coupling were fitted analytically to functional forms to obtain a permutationally invariant 2×2 diabatic potential-energy matrix. An analytic representation of the adiabatic potential-energy surfaces is then obtained by diagonalizing the diabatic potential-energy matrix. The analytic representation of the surfaces gives an analytic representation of the four-dimensional conical intersection seam which is discussed in detail. © *2006 American Institute of Physics*.
[DOI: 10.1063/1.2168447]

I. INTRODUCTION

The electronically excited states and photochemistry of ammonia have been studied extensively both theoretically[1–9] and experimentally.[10–30] Photodissociation of ammonia through the first singlet excited ($\tilde{A}\ ^1A_2''$) state is a prototype problem for nonadiabatic dynamics. The electronic ground state ($\tilde{X}\ ^1A_1$) has two C_{3v} minima connected by a low-frequency inversion mode with a D_{3h} saddle point. The excited state is quasibound with a trigonal planar D_{3h} minimum and a C_{2v} transition state in the N–H dissociation channel leading to NH_2+H products. The ground electronic state has a conical intersection with the $\tilde{A}$ excited singlet electronic state, leading to competition between the adiabatic and nonadiabatic NH_2+H pathways for dissociation:

$$NH_3(\tilde{A}\ ^1A_2'') \rightarrow \begin{cases} NH_2(\tilde{X}\ ^2B_1) + H & \text{(dissociation 1)}, \\ NH_2(\tilde{A}\ ^2A_1) + H & \text{(dissociation 2)}. \end{cases}$$

The ground electronic state of the NH_2 products ($^2B_1$) correlates diabatically with the first excited ($^1A_2''$) state of NH_3, while the first excited state of NH_2 products ($^2A_1$) correlates diabatically with the ground state ($^1A_1$) of ammonia. For general planar geometries, the symmetry of the $^1A_1$ ground state becomes $^1A'$, the symmetry of the $^1B_1$ state becomes $^1A''$, and the adiabatic potential-energy surfaces cross at a four-dimensional conical intersection seam. (For the one-dimensional subspace the symmetries become $^1A_1'$ and $^1A_2''$, respectively.) However, in general nonplanar geometries both the $^1A'$ ($^1A_1'$) and the $^1A''$ ($^1A_2''$) states have the same ^1A symmetry, and nonplanar geometries have avoided crossings. The topographies of these coupled potential-energy surfaces are critical for the photofragmentation dynamics of the $\tilde{A}$ state, which has been studied in recent state-selective experiments.[25–30]

In the present study we present coupled potential-energy surfaces for simulating the photofragmentation process. Traditionally, potential-energy surfaces are generated by computing the eigenstates of an electronic Hamiltonian for a grid of nuclear geometries and fitting the energies to a function of the nuclear coordinates. The coupling between the adiabatic potential-energy surfaces, which is needed for dynamical calculations, can then be obtained by calculating nuclear momentum matrix elements between the eigenstates. This vector coupling (commonly referred to as the nonadiabatic coupling) is a function of nuclear coordinates that can be rapidly varying in the regions of avoided crossings and singular at conical intersections.[31,32] When fitting surfaces in the adiabatic representation, it is difficult to ensure that singularities occur where the adiabats cross and that the slopes of the upper and lower adiabats are consistent at the multidimensional crossing, where these slopes are discontinuous.

Recently, a promising alternative was presented; this involves directly computing diabatic states based on configurational uniformity.[33–36] Diabatic states can be defined as states whose nuclear momentum vector coupling terms are negligibly small.[32] Strict diabatic states where these terms are zero do not exist in general since the nuclear momentum coupling terms cannot be made to simultaneously vanish in all nuclear coordinates over a finite region of space,[37] and therefore diabatic states are sometimes called quasidiabatic states, but we will use the shorter notation. In fact, one may divide the nuclear momentum coupling into a transverse part that cannot be transformed away and longitudinal part that can be.[37] The transverse part is not only nonzero in all representations, but far from a conical intersection it is not even smaller, in general, than the longitudinal part.[37,38] However, we can find diabatic bases where the nuclear momentum

[a]Electronic mail: nangia@t1.chem.umn.edu

coupling is everywhere as small in order of magnitude as it is in conventional Born-Oppenheimer situations in which the ground state is widely separated from all the excited states.[32,38] Therefore, neglecting nuclear momentum coupling in such diabaticbases has the same validity as making the Born-Oppenheimer approximation when there are no low-lying states.[38] There is no unique way to find such diabatic states, but we will use the recently proposed fourfold way,[34–36] which involves first using multiconfiguration quasidegenerate perturbation theory (MC-QDPT),[39,40] then transforming to diabatic states on the basis of configurational uniformity.[33,34] Although the inconvenient nuclear momentum coupling can be neglected in a diabatic representation, the states are still coupled. However, the diabatic coupling is a smooth, nonsingular, scalar function and it is much more convenient to handle in dynamics calculations. The fourfold-way diabatization scheme is called direct because, unlike most previous methods for finding diabatic states,[33,34] the fourfold way does not require following a path through configuration space.

This paper is organized as follows. The details of the *ab initio* calculations are described in Sec. II. The functional forms for fitting the six-dimensional diabatic surfaces and couplings are presented in Sec. III. Section IV includes a discussion of the quality of the fit and the procedure of diagonalizing the diabatic matrix to obtain adiabatic states. The conclusions are provided in Sec. V.

II. *AB INITIO* ELECTRONIC STRUCTURE CALCULATIONS

The diabatization scheme is presented in detail in previous papers.[34–36] In Sec. II.A, we summarize the key concepts and introduce the terminology to be used, and in Sec. II.B, we present the application of the general scheme to ammonia.

II.A. Summary of the diabatization procedure and theory

The two lowest-energy diabatic states ϕ_1 and ϕ_2 are obtained by an orthogonal transformation of the two lowest adiabatic states ψ_1 and ψ_2:

$$\phi_k = \sum_{n=1}^{2} T_{nk}\psi_n, \tag{1}$$

where T_{nk} is an element of the adiabatic/diabatic transformation matrix. Each adiabatic state is expressed as a linear combination of L orthonormal configuration state functions (CSFs) denoted by χ_α:

$$\psi_n = \sum_{\alpha=1}^{L} C_{\alpha n}\chi_\alpha, \tag{2}$$

where $C_{\alpha n}$ is determined by a perturbation-theory calculation. In particular, we use multiconfiguration quasidegenerate perturbation theory[39,40] based on a complete active space self-consistent-field[41] (CASSCF) reference state. The CSFs are symmetry-adapted combinations of the Slater determinants built from canonical CASSCF molecular orbitals.

The first step in the diabatization scheme is to define the weak-interaction regions and identify the potential reference geometries, i.e., geometries where the adiabatic states are well separated in energy, and the nonadiabatic coupling is negligible, so that the adiabatic states are found to be good approximations to the diabatic states. A potential reference geometry $\mathbf{Q}^{\mathrm{ref}}$ is expected to be dominated by a small number of CSFs that are assumed to be good prototypes for the diabatic states. The diabatic prototypes are required to have the following properties. (1) Each diabatic state ϕ_k should be dominated by a unique group of CSFs called G_k. (2) The group list G_k should remain the same for all nuclear geometries.

A potential reference geometry that is used to determine the dominant CSF list is called a reference geometry. A system with more than one product arrangement requires reference geometries in each arrangement, and a consistent dominant CSF list for the entire system for all nuclear geometries is obtained by combining the CSF lists of all the reference geometries in each arrangement.[35] For the present application to NH_3, as discussed further below, we used six reference geometries.

A key aspect of the diabatization procedure is configurational uniformity. Since diabatic states are smooth functions of coordinates, the molecular orbitals (MOs) participating in the dominant CSFs that define the diabatic prototypes should deform smoothly along paths in the nuclear coordinate space. Such smoothly varying MOs are called diabatic molecular orbitals (DMOs).

The determination of DMOs from the canonical CASSCF adiabatic MOs u_μ used in the CSFs is carried out by a systematic and general scheme called the fourfold way.[34–36] The first step of the fourfold way is the maximization of threefold density criterion defined as

$$D_3(\alpha_N, \alpha_R, \alpha_T) = 2D^{\mathrm{NO}} + D^{\mathrm{ON}} + 0.5D^{\mathrm{TD}}. \tag{3}$$

The functionals D^{NO}, D^{ON}, and D^{TD} in Eq. (3) are the natural orbital, occupation number, and the transition density terms, respectively. More specifically, the natural orbital functional is defined as

$$D^{\mathrm{NO}} = N\sum_{\mu=1}^{\eta} (\bar{p}_{\mu\mu})^2, \tag{4}$$

where η is the number of MOs that are used to construct CSFs, N is the number of diabatic states, and $\bar{\mathbf{p}}$ is a state-averaged density matrix given as

$$\bar{\mathbf{p}} = \frac{1}{N}\sum_{n=1}^{N} \mathbf{p}^n, \tag{5}$$

where $\boldsymbol{p}^n$ is a matrix with elements $p^n_{\mu\nu}$, which is the one-particle density-matrix element of the adiabatic wave function ψ_n, and μ and ν are the molecular-orbital labels. The occupation number functional is defined as

$$D^{\mathrm{ON}} = \sum_{\mu=1}^{\eta}\sum_{n=1}^{N} (p^n_{\mu\mu})^2. \tag{6}$$

Finally, the transition density functional is defined as

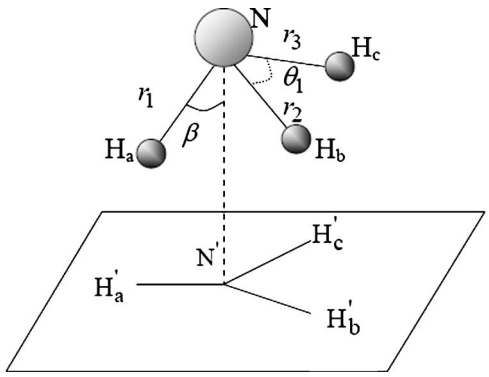

FIG. 1. Internal coordinates used for fitting diabatic potential-energy surfaces and nonadiabatic coupling. The N–H bond distances are shown by r_1, r_2, and r_3, and the H–N–H bond angles are shown by θ_1, θ_2, and θ_3. NN′ is the trisector direction, and β is the angle between the any N–H bond and NN′. The prime denotes the projection of the atoms on a plane perpendicular to the NN′ direction.

$$D^{\mathrm{TD}} = \frac{2}{N-1} \sum_{\mu=1}^{\eta} \sum_{m<n}^{N} (p_{\mu\mu}^{mm})^2, \tag{7}$$

where $\mathbf{p}^{mn}$ is the transition density matrix between adiabatic states ψ_m and ψ_n. The maximization of the D_3 functional at a reference geometry allows us to find DMOs in which to reexpress the CSFs. For the present application to NH_3, $\eta = 102$ and $N=2$.

Since the reference geometries are chosen in weak-interaction regions, the DMOs identified by the threefold criterion need not to remain smooth in the strong-interaction regions. A fourth criterion involving maximum overlap reference MOs (MORMOs) is therefore applied in addition to the threefold density criterion. For this purpose a subset of the DMOs is selected as reference MOs, which is denoted as u_τ^{ref}, $\tau = 1, 2, \ldots, \lambda$. These reference MOs are used to calculate the reference overlap functional D^{RO} given by

$$D^{\mathrm{RO}} = \sum_{\tau=1}^{\lambda} \{\sigma_{\tau\tau}(\mathbf{Q}, \mathbf{Q}_\lambda^{\mathrm{ref}})\}^2, \tag{8}$$

where $\sigma_{\tau\tau}(\mathbf{Q}, \mathbf{Q}^{\mathrm{ref}})$ is an overlap quantity[34] involving orbital u_τ at an arbitrary geometry $\mathbf{Q}$ and u_τ at the reference geometry $\mathbf{Q}^{\mathrm{ref}}$. For the present application to NH_3, $\lambda = 1$.

II.B. Computational procedure

The 6-31++G($3df, 3pd$) basis set[42,43] is used for the calculations, which are carried out using the HONDOPLUS, v.4.5 (Refs. 44 and 45) electronic structure package. The active space consists of seven orbitals with eight electrons, which corresponds for NH_3 to a full valence active space. In the MC-QDPT step, one inactive orbital corresponding to the $1s$ core orbital of N was frozen (that is kept doubly occupied in all CSFs), and the perturbation includes electronic excitation from all of the active orbitals through second order.

Figure 1 shows the internal coordinate system with the three N–H internuclear distances r_1, r_2, and r_3; a trisector angle β, defined as an angle that any of the N–H bond axes makes with the NN′ trisector direction; θ_1, θ_2, and θ_3 are the H–N–H bond angles. The trisector angle varies in the range $0 \leqslant \beta \leqslant \pi$, and $\beta = \pi/2$ denotes a planar ammonia geometry. (The use of the trisector angle as an internal coordinate was suggested in earlier studies[46–49] in which the ground-state potential-energy surface was fit.) The internal coordinates are represented as $\mathbf{Q} = r_1, r_2, r_3, \theta_1, \theta_2, \theta_3$, and β. Note that we use seven internal coordinates, so one of them is redundant; this does not cause any problem and in fact the use of all seven of the coordinates makes it easier to impose permutational symmetry than it would be if one of the θ_i was omitted.

We are interested in photodissociation of ammonia to form NH_2+H products, and we have not considered the fragmentation of NH_3 to NH+H_2 or NH+2H products in this study. As in the case of multiarrangement reactions, more than one reference geometry are required, and we used six reference geometries. Reference geometries $\mathbf{Q}_i^{\mathrm{ref}}$ $(r_1, r_2, r_3, \theta_1, \theta_2, \theta_3, \beta)$ were chosen with at least one in each of the asymptotic regions for dissociation of each of the three H atoms, and they include both planar and nonplanar geometries, in particular,

$$\begin{aligned}
\mathbf{Q}_1^{\mathrm{ref}} &= (5.0, 1.1, 1.1, 2\pi/3, 2\pi/3, 2\pi/3, \pi/2),\\
\mathbf{Q}_2^{\mathrm{ref}} &= (1.1, 5.0, 1.1, 2\pi/3, 2\pi/3, 2\pi/3, \pi/2),\\
\mathbf{Q}_3^{\mathrm{ref}} &= (1.1, 1.1, 5.0, 2\pi/3, 2\pi/3, 2\pi/3, \pi/2),\\
\mathbf{Q}_4^{\mathrm{ref}} &= (5.0, 1.1, 1.1, 2\pi/3, 2\pi/3, 2\pi/3, \pi/6),\\
\mathbf{Q}_5^{\mathrm{ref}} &= (5.0, 1.1, 1.1, 2\pi/3, 5\pi/6, \pi/2, \pi/3),\\
\mathbf{Q}_6^{\mathrm{ref}} &= (5.0, 1.1, 1.1, \pi, \pi/2, \pi/2, \pi/3),
\end{aligned} \tag{9}$$

where distances are in angstroms. The reference geometries in different asymptotic regions have different diabatic prototypes. For example, $\mathbf{Q}_1^{\mathrm{ref}}$ has DMOs localized on $H_a + H_b NH_c$, whereas $\mathbf{Q}_2^{\mathrm{ref}}$ has DMOs on $H_b + H_a NH_c$. Similar relationships exist between other reference geometries; therefore it is important to establish a one-to-one correspondence between them in order to make a consistent dominant CSF list. The procedure used is summarized here: (1) With initial geometry $\mathbf{Q}$ equal to $\mathbf{Q}_1^{\mathrm{ref}}$, we carry out a threefold density calculation and find the DMOs $u_\tau(\mathbf{Q})$. (2) Then we select another geometry $\mathbf{Q}'$ close to $\mathbf{Q}$ and find the DMOs $u_\tau(\mathbf{Q}')$ and identify a one-to-one correspondence between the DMOs at the two geometries. (3) With the $\mathbf{Q}'$ now labeled consistently with $\mathbf{Q}$ we repeat step (2) with geometries $\mathbf{Q}'$ successively translated in small steps until $\mathbf{Q}_2^{\mathrm{ref}}$ is reached.

This establishes one-to-one correspondence between the set of DMOs $u_\tau(\mathbf{Q}_1^{\mathrm{ref}})$ and $u_\tau(\mathbf{Q}_2^{\mathrm{ref}})$ for these two geometries. We follow steps (1)–(3) starting at $\mathbf{Q}_1^{\mathrm{ref}}$ and connect it to $\mathbf{Q}_{3,\ldots,6}^{\mathrm{ref}}$ in order to establish correspondence between $u_\tau(\mathbf{Q}_{1,\ldots,6}^{\mathrm{ref}})$ DMOs at all six reference geometries. Since the DMOs obtained should be independent of the path followed in steps (1)–(3) we test the correspondence by following different intermediate paths to connect the reference geometries. As mentioned above, different reference geometries will have different characters and different sets of DMOs, and this can lead to a CSF grouping problem. It was found

that some of the DMOs in planar reference geometries (i.e., $\mathbf{Q}_1^{\mathrm{ref}}$, $\mathbf{Q}_2^{\mathrm{ref}}$, and $\mathbf{Q}_3^{\mathrm{ref}}$) were missing from the nonplanar reference geometries ($\mathbf{Q}_4^{\mathrm{ref}}$, $\mathbf{Q}_5^{\mathrm{ref}}$, and $\mathbf{Q}_6^{\mathrm{ref}}$). To obtain a consistent CSF list for all six reference geometries we took a union of all CSFs obtained at each reference geometry. The final dominant CSF lists for the diabatic states ϕ_1 and ϕ_2 are $G_1=\{\chi_1,\chi_2,\chi_3\}$ and $G_2=\{\chi_4,\chi_5,\chi_6\}$, respectively. Each χ_α is defined by seven valence molecular orbitals u_τ, where the electronic configuration of each χ_α is as follows:

$$\begin{aligned}
&\chi_1:(u_1)^2(u_2)^2(u_3)^2(u_4)^2(u_5)^0(u_6)^0(u_7)^0,\\
&\chi_2:(u_1)^2(u_2)^2(u_3)^1(u_4)^2(u_5)^1(u_6)^0(u_7)^0,\\
&\chi_3:(u_1)^2(u_2)^2(u_3)^2(u_4)^0(u_5)^2(u_6)^0(u_7)^0,\\
&\chi_4:(u_1)^2(u_2)^2(u_3)^2(u_4)^1(u_5)^1(u_6)^0(u_7)^0,\\
&\chi_5:(u_1)^2(u_2)^2(u_3)^1(u_4)^1(u_5)^2(u_6)^0(u_7)^0,\\
&\chi_6:(u_1)^2(u_2)^1(u_3)^2(u_4)^2(u_5)^1(u_6)^0(u_7)^0.
\end{aligned} \tag{10}$$

These lists do not include the doubly occupied core orbital on N, and the valence u_τ are numbered in order of increasing orbital energy.

III. FIT TO THE DIABATIC POTENTIAL-ENERGY SURFACES

The diabatic electronic states ϕ_1 and ϕ_2 and the matrix elements of the electronic Hamiltonian in the diabatic representation are

$$U_{11}=\langle\phi_1|H_{\mathrm{el}}|\phi_1\rangle, \tag{11}$$

$$U_{22}=\langle\phi_2|H_{\mathrm{el}}|\phi_2\rangle, \tag{12}$$

$$U_{12}=\langle\phi_1|H_{\mathrm{el}}|\phi_2\rangle, \tag{13}$$

where the off-diagonal term is the diabatic coupling term. Note that, following the standard convention, H_{el} includes the nuclear repulsion. The electronic Hamiltonian expressed in the diabatic basis is a 2×2 matrix of

$$\mathbf{U}=\begin{bmatrix} U_{11}(\mathbf{Q}) & U_{12}(\mathbf{Q}) \\ U_{12}(\mathbf{Q}) & U_{22}(\mathbf{Q}) \end{bmatrix}, \tag{14}$$

where $\mathbf{Q}$ is the set of nuclear coordinates as defined in Sec. II.B. Since the electronic Hamiltonian provides the potential-energy surfaces on which the nuclei move, the $\mathbf{U}$ matrix is also known as the diabatic potential-energy matrix. The MC-QDPT method was used to generate U_{11}, U_{22}, and U_{12} at 3600 geometries. The nuclear geometries were chosen to form a grid in six dimensions such that $r_1=0.8,1.02,1.5,2.0$, and 5.0 Å; r_2 and $r_3=0.8,1.02$, and 1.5 Å; θ_1, θ_2, and $\theta_3=\pi/3,\pi/2,2\pi/3$, and $5\pi/6$; $\beta=\pi/12,\pi/6,\pi/4,\pi/3$, and $\pi/2$. This includes 720 geometries with one H atom 5 Å from NH_2, plus 720 geometries corresponding to planar NH_3 and 2160 points corresponding to nonplanar NH_3.

There are three identical hydrogen atoms in ammonia, and the fitted diabatic potential-energy matrix should be invariant to the labeling of the three hydrogen atoms. In the present study, we incorporated permutation symmetry between the three hydrogen atoms by introducing a symmetrizing operator, which is described in Sec. III.A. During the fitting procedure, the symmetrizer operates on all the matrix elements of $\mathbf{U}$.

III.A. Symmetrizer

The group of all possible permutations involving the hydrogen atoms in ammonia is the symmetric group S_3. There are six permutation operations in S_3, the identity operator $\mathbf{e}$, three transposition operators, and two cyclic operators.[50] The transposition operators are of the form $\mathbf{p}_{ij}$ with $i,j=1,\ldots,3$; $i<j$, and they involve switching any two hydrogen atoms while keeping the third one fixed. The final two permutation operators are cyclic permutations of the form $\mathbf{p}_{ijk}$ with $i\neq j\neq k$. To represent the six permutations in a compact notation, we will introduce a generic $\mathbf{p}_\alpha$ such that

$$\mathbf{p}_\alpha=\{1,12,13,23,123,321\}; \tag{15}$$

thus $\alpha=1,2,\ldots,6$ denotes the six permutations. Each of the six permutation operators can be represented as a 3×3 matrix, and the matrix representations of the operators are given in supporting information.[51] Note that $\mathbf{p}_\alpha$ is a number operator and operates on the indices of the three hydrogen atoms. The representation of the permutation operator in terms of the internal coordinate $\mathbf{Q}$ is denoted as $\mathbf{P}_\alpha$. The operator $\mathbf{P}_\alpha$ operates on the seven-dimensional vector $\mathbf{Q}$ and is represented using a 7×7 matrix. The matrix representation of $\mathbf{P}_\alpha$ is expressed by the following direct sum:

$$\mathbf{P}_\alpha=\mathbf{p}_\alpha\otimes\mathbf{p}_\alpha\oplus\mathbf{I}_1, \tag{16}$$

and has the form

$$\mathbf{P}_\alpha=\left[\begin{array}{c|c|c} \begin{matrix} r\text{ block}\\ \mathbf{p}_\alpha\\ 3\times 3\end{matrix} & \mathbf{0} & \\ \hline \mathbf{0} & \begin{matrix}\theta\text{ block}\\ \mathbf{p}_\alpha\\ 3\times 3\end{matrix} & \\ \hline & & \mathbf{I}_1 \end{array}\right], \tag{17}$$

where $\mathbf{I}_1$ is the identity matrix in one dimension. The symmetrizer $\mathbf{S}$ is defined as a $(3!)^{-1}$ times a sum over all $\mathbf{P}_\alpha$:

$$\mathbf{S}=\frac{1}{6}\sum_\alpha\mathbf{P}_\alpha=\frac{1}{6}[\mathbf{e}+\mathbf{P}_{12}+\mathbf{P}_{13}+\mathbf{P}_{23}+\mathbf{P}_{123}+\mathbf{P}_{321}]. \tag{18}$$

III.B. U_{11} surface

The lower-energy diabatic surface was fitted with the symmetrized functional form

$$U_{11}(\mathbf{Q})=\sum_{\substack{i\leq j\leq k\\ l\leq m\leq n\\ p}} C^{(1)}_{ijklmnp}\sum_\alpha A^{(1)}_{ijklmnp}(\mathbf{P}_\alpha\mathbf{Q}), \tag{19}$$

where

$$A^{(\omega)}_{ijklmnp}(\mathbf{Q}) = f_\omega(r_1)^i f_\omega(r_2)^j f_\omega(r_3)^k g_\omega(\theta_1,r_2,r_3)^l \times g_\omega(\theta_2,r_1,r_3)^m g_\omega(\theta_3,r_1,r_2)^n h(p,\beta), \quad (20)$$

where

$$f_\omega(r) = 1 - [\kappa_\omega e^{-\gamma_\omega(r-r_{o\omega})}], \quad (21)$$

$$g_\omega(\theta_a,r_b,r_c)^l = (\theta-\theta_{o\omega})^l e^{-\delta_\omega(r_b^2+r_c^2)} + \eta^l_\omega(1-e^{-\delta_\omega(r_b^2+r_c^2)}) \quad [a,b,c=1,2,3;a\neq b\neq c], \quad (22)$$

$$h(p,\beta) = \cos\left[p\left(\beta-\frac{\pi}{2}\right)\right], \quad (23)$$

with $0\leqslant i,j,k\leqslant 2$, $0\leqslant l,m,n\leqslant 2$, and $0\leqslant p\leqslant 4$. Note that if p were restricted to $p=0$, then Eq. (19) would be a six-dimensional multinomial, but p is a Fourier cosine series coefficient, not a power. For cases with $p<4$, the constraints in the indices are $i+j+k\leqslant 4$ and $l+m+n\leqslant 2$. For $p=4$, $i+j+k\leqslant 4$, $l+m+n\leqslant 2$, and $i+j+k+l+m+n\leqslant 0$. There are total of 127 coefficients for $\omega=1$. The values of the coefficients were obtained by linear squares fitting routine for given values of nonlinear parameters (discussed in the next paragraph) and are provided in the supporting information.[51]

The function f_ω in Eqs. (20) and (21) is a Morse function, and powers of this function are used to describe each of the three N–H stretches. The r_{o1} parameter in Eq. (21) corresponds to the ground-state equilibrium N–H distance, and the γ_1 parameter was optimized manually to obtain a minimum root-mean-square (rms) deviation of the fit from the data. The parameters are given in the supporting information.[51] The bend displacement about each angular coordinate (in radians) is described by the g_ω function. The presence of Gaussian functions in g_ω ensures that in the dissociation limit the bending terms associated with the breaking bond vanish for the product geometry. The inversion coordinate is symmetric about the D_{3h}, geometry and is therefore described by a cosine function with a $\pi/2$ reference angle.

The shape of the U_{11} surface was found to be very important for describing key features of the ground adiabatic surface such as the equilibrium geometry, the saddle-point geometry for inversion, and the inversion barrier height. For fitting U_{11}, the 47 geometries with energies less than or equal to 0.5 eV were weighted higher than the other 3553 geometries by a factor of 5. This allowed us to obtain a better fit in the regions that are most important for the experiments of Refs. 10–30.

III.C. U_{22} surface

The higher-energy diabatic surface $U_{22}(\mathbf{Q})$ was represented as the eigenvalue of a 2×2 matrix of the form

$$W = \begin{bmatrix} W_{11}(\mathbf{Q}) & W_{12}(\mathbf{Q}) \\ W_{12}(\mathbf{Q}) & W_{22}(\mathbf{Q}) \end{bmatrix}, \quad (24)$$

where the matrix elements are all fitting functions. The lowest root is

$$U_{22}(\mathbf{Q}) = \tfrac{1}{2}[(W_{22}+W_{11}) - \sqrt{(W_{22}-W_{11})^2+4W_{12}^2}]. \quad (25)$$

The diagonal matrix elements in Eq. (24) were determined by simultaneous least-squares fits. The functional form of the symmetrized $W_{11}(\mathbf{Q})$ surface is given as

$$W_{11}(\mathbf{Q}) = \sum_{\substack{i\leqslant j\leqslant k\\ l\leqslant m\leqslant n\\ p}} C^{(2)}_{ijklmnp} \sum_\alpha A^{(2)}_{ijklmnp}(\mathbf{P}_\alpha\mathbf{Q}), \quad (26)$$

with $0\leqslant i,j,k\leqslant 2$, $0\leqslant l,m,n\leqslant 2$, and $0\leqslant p\leqslant 4$ with additional constraints $i+j+k\leqslant 4$, $l+m+n\leqslant 2$, and $i+j+k+l+m+n>0$. We set δ_2 and η_2 equal to δ_1 and η_1, respectively. The functional form of the symmetrized $W_{22}(\mathbf{Q})$ surface is given as

$$W_{22}(\mathbf{Q}) = \sum_{\substack{i\leqslant j\leqslant k\\ l\leqslant m\leqslant n\\ p}} C^{(3)}_{ijklmnp} \sum_\alpha A^{(3)}_{ijklmnp}(\mathbf{P}_\alpha\mathbf{Q}), \quad (27)$$

with the same upper limits and as for $W_{11}(\mathbf{Q})$. We set δ_3 and η_3 equal to δ_1 and η_1, respectively. The off-diagonal coupling $W_{12}(\mathbf{Q})$ is fixed at 0.8 eV for all geometries. The U_{22} surface was constructed by first fitting the two W_{11} and W_{22} surfaces and then calculating U_{22} using Eq. (25).

The use of a multiconfigurational representation involving the W_{11} and W_{22} surfaces was motivated by the need to fit features such as the excited-state minimum and the saddle point for dissociation on the U_{22} surface. To better describe the region of conical intersection and the saddle point for the dissociation 772 geometries with U_{22} in the range of 4–6 eV were given a weight of 3 for fitting both W_{11} and W_{22}, and the remaining 2828 geometries were given a weight of unity. The lists of 124 coefficients and the new nonlinear parameters for $\omega=2$ and $\omega=3$ are provided in the supporting information.[51]

III.D. U_{12} surface

The nonadiabatic coupling obtained by the diabatization procedure was fitted using the following symmetrized functional form:

$$U_{12}(\mathbf{Q}) = \sum_{\substack{i\leqslant j\leqslant k\\ l\leqslant m\leqslant n\\ p}} C^{(4)}_{ijklmnp} \sum_\alpha B^{(4)}_{ijklmnp}(\mathbf{P}_\alpha\mathbf{Q}), \quad (28)$$

where $B_{ijklmnp}(\mathbf{Q})$ has the form

$$B_{ijklmnp}(\mathbf{Q}) = r_1^i r_2^j r_3^k F(r_1)F(r_2)F(r_3)\theta_1^l\theta_2^m\theta_3^n G(p,\beta), \quad (29)$$

where

$$F(r) = 1 - 0.5\tanh[(r-r_{o4})], \quad (30)$$

$$G(p,\beta) = \sin\left[p\left(\beta-\frac{\pi}{2}\right)\right], \quad (31)$$

where $0\leqslant i,j,k\leqslant 2$ and $0\leqslant l,m,n\leqslant 2$ with additional constraints $i+j+k\leqslant 2$, $l+m+n\leqslant 2$, and $i+j+k+l+m+n>0$; and where r_{o4} is listed in the supporting information.[51] In the present fit we used $3\leqslant p\leqslant 5$ because this choice yields a better fit and lower rms deviation of errors than $1\leqslant p\leqslant 3$.

TABLE I. Mean unsigned deviation of the fitted U_{11} energies from their mean value for several energy ranges.

U_{11} (eV)	N[a]	Mean unsigned deviation (eV)
0–1	75	0.02
0–2	84	0.05
0–3	132	0.07
0–4	208	0.09
0–5	354	0.09
0–6	534	0.11
0–7	922	0.12
0–8	1325	0.15
0–9	1785	0.17
0–10	2223	0.20

[a]N is the number of points in the indicated energy range.

TABLE II. Mean unsigned deviation of the fitted U_{22} energies from their mean value for several energy ranges.

U_{22} (eV)	N[a]	Mean unsigned deviation (eV)
0–5	265	0.09
0–6	507	0.09
0–7	1134	0.10
0–8	1554	0.12
0–9	2166	0.15
0–10	2671	0.19
0–11	2995	0.21
0–12	3175	0.21
0–13	3329	0.23
0–14	3411	0.25

[a]N is the number of points in the indicated energy range.

With either choice, U_{12} is linear in $(\beta-\pi/2)$ for values close to $\pi/2$.

A key element of the present direct procedure is that U_{12} is obtained directly from the diabatization then fit independently of U_{11} and U_{22}, whereas in indirect procedures it is sometimes fit to minimize the errors in the adiabatic surfaces. (Our fitting procedure does not use the adiabatic surface at all.) The least-squares fit for U_{12} was carried out with a uniform unit weight for all geometries. A list of 45 nonzero unique coefficients that were optimized by minimizing the rms deviation from the MC-QDPT values is provided in the supporting information.[51]

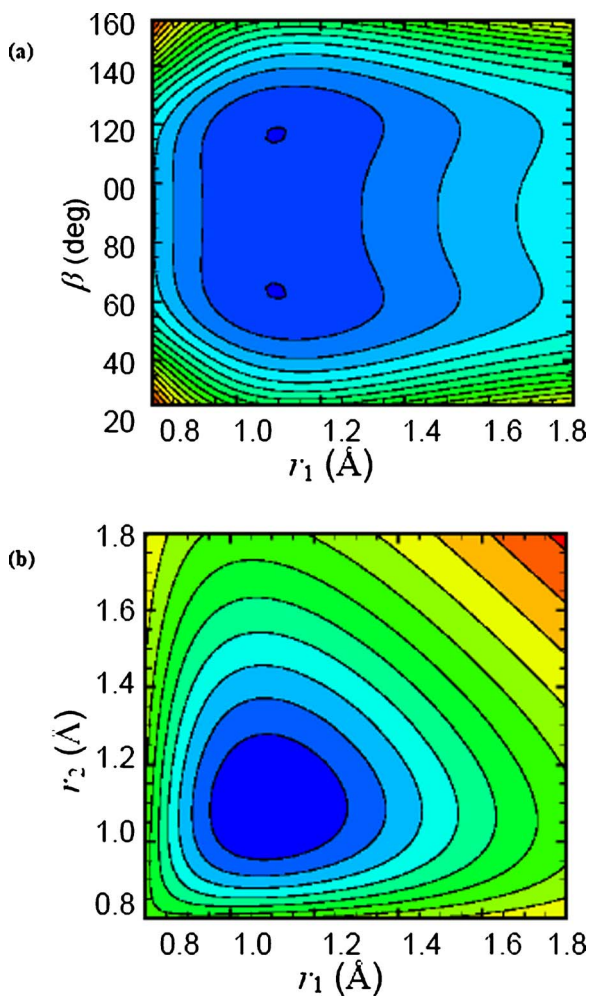

FIG. 2. (Color online) Contour plots of the U_{11} potential-energy surface of ammonia along (a) N–H stretch r_1 and the inversion angle β and (b) two N–H stretches r_1 and r_2. For each plot all other degrees of freedom are fixed at the equilibrium ground-state geometry of ammonia. The contour spacing is 0.5 eV.

III.E. Availability

The fitted surfaces, including analytic gradients in Cartesian coordinates, have been deposited in the POTLIB[52,53] potential-energy surface library, where they are freely available to all interested parties.

IV. DISCUSSION

The mean unsigned error (MUE) of the fit to U_{11} is tabulated as a function of energy in Table I, where the zero of energy throughout this article is the equilibrium geometry of ground-state NH_3. For energies below 1 eV the fit agrees

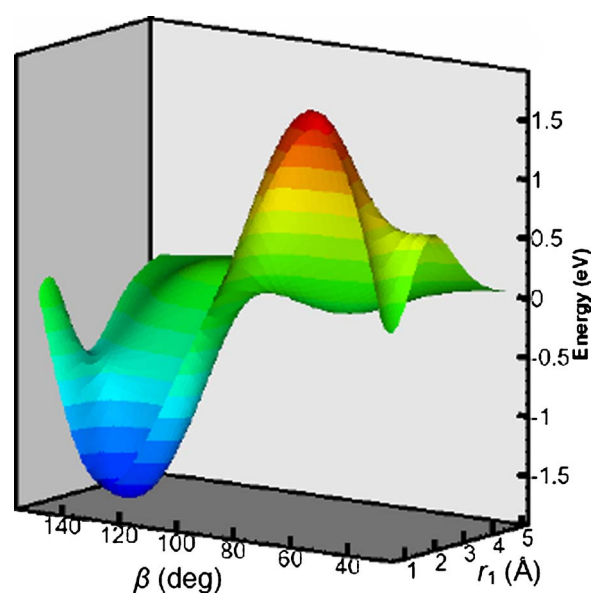

FIG. 3. (Color online) Three-dimensional plot of the U_{12} potential-energy surfaces for ammonia along the N–H stretch r_1 and the inversion angle β. All other coordinates were fixed at the equilibrium geometry. The coupling term goes to zero at $\beta=\pi/2$ and is positive for $\beta<\pi/2$ and negative for $\beta>\pi/2$.

TABLE III. Mean unsigned deviation of the fitted U_{12} energies from their mean value for several energy ranges.

$\lvert U_{12}\rvert$ (eV)	N[a]	Mean unsigned deviation (eV)
0–0.25	2247	0.01
0–0.50	3077	0.01
0–0.75	3219	0.01
0–1.00	3337	0.01
0–1.25	3416	0.01
0–1.50	3485	0.02
0–1.75	3528	0.02
0–2.00	3600	0.02

[a]N is the number of points in the indicated energy range.

with the *ab initio* data within 0.02 eV, on average. For higher-energy geometries, but still below the dissociation limit (~5 eV), the MUE of the fit is 0.1 eV. We consider this to be good agreement between the data and the fit, since the fit is a global one spanning energies from the minimum to far above the dissociation limit of ammonia. Figure 2(a) shows the contours of the U_{11} surface near the minimum as a function of the N–H stretch r_1 and inversion angle β with other coordinates fixed at $r_2=r_3=1.020$ Å and $\theta_1=\theta_2=\theta_3=107.5°$. The plot shows the location of two C_{3v} minima at $r_1=1.02$ Å and $\beta=67.5°$ and 112.5°. The two minima are separated by an inversion barrier of 0.25 eV at the planar D_{3h} geometry with $r_1=1.02$ Å and $\beta=\pi/2$. Figure 2(b) shows the contours of the U_{11} surface along r_1 and r_2 with other coordinates fixed at $r_3=1.02$ Å, $\theta_1=\theta_2=\theta_3=107.5°$, and $\beta=67.5°$. The lowest-energy contour shows the minimum in U_{11} at the C_{3v} geometry with $r_2=r_3=1.02$ Å.

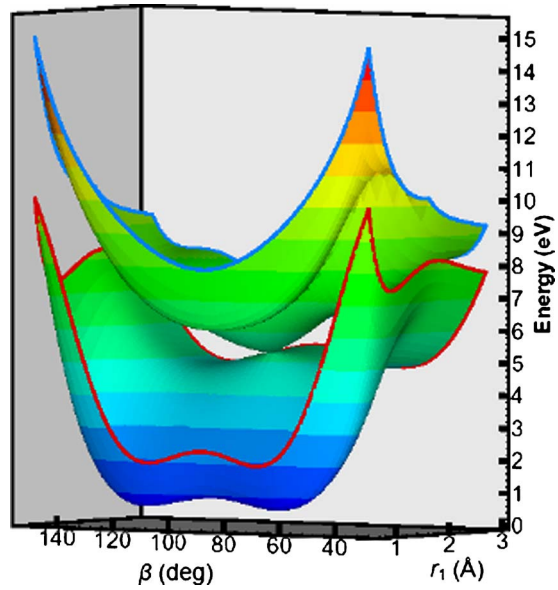

FIG. 5. (Color online) Three-dimensional plot of adiabatic potential-energy surfaces for ammonia up to the dissociation limit of r_1 and over a wide range of the inversion angle β. The conical intersection appears at $\beta=\pi/2$, and all other coordinates were fixed at the equilibrium geometry. The contour spacing is 1 eV.

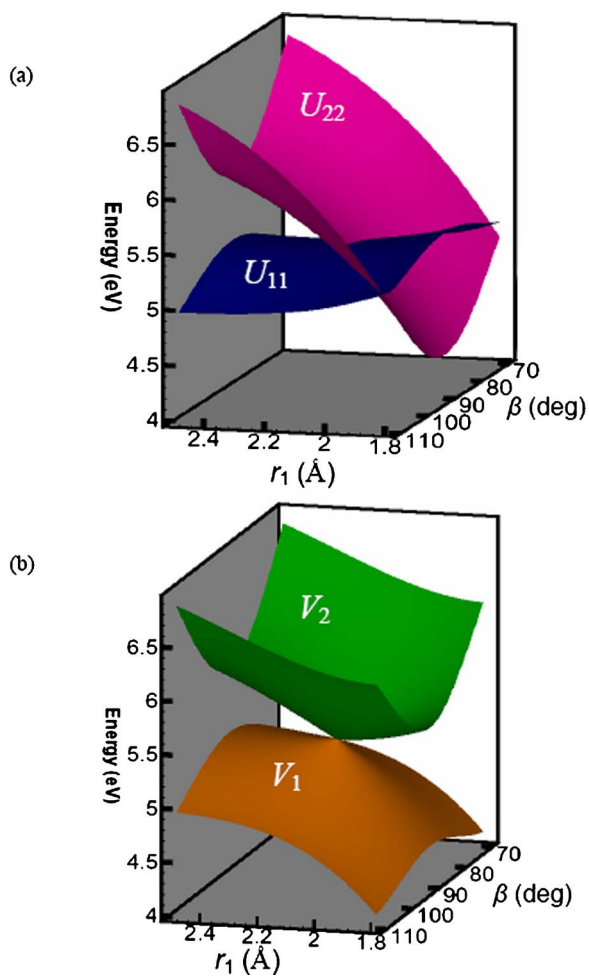

FIG. 4. (Color online) Three-dimensional plots of (a) the U_{11} and U_{22} diabatic potential-energy surfaces showing the diabatic crossing of the two surfaces and (b) the V_1 and V_2 adiabatic potential-energy surfaces of ammonia showing the conical intersection along the N–H stretch r_1 and the inversion angle β. The conical intersection forms at $r_1=2.13$ Å and $\beta=\pi/2$ with all other coordinates fixed at the equilibrium geometry.

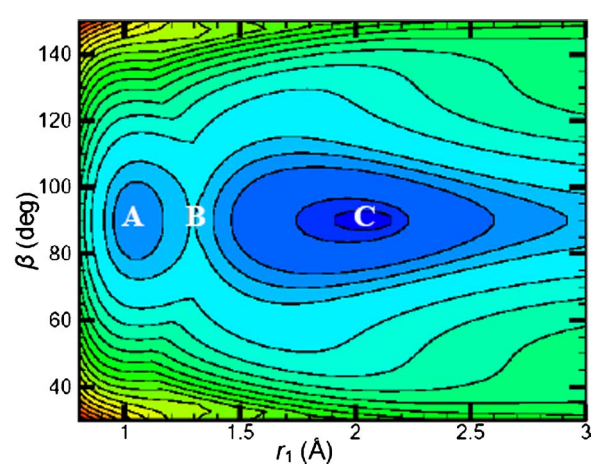

FIG. 6. (Color online) Contour plot of V_2 adiabatic potential-energy surface of ammonia. On the plot the excited-state minimum-energy point is labeled as A, and the geometry of the conical intersection is labeled as C. The saddle point of the dissociation channel is labeled as B. The contour spacing is 0.5 eV.

TABLE IV. Key features of the fitted adiabatic surfaces.

Quantity	Present fit	Best previous estimate(s)			Experiment
V_1					
Equilibrium geometry (Å and deg)					
r_1	1.010	1.011[a]	1.011[b]	1.013[c]	
θ_1	108.4	106.8[a]	106.7[b]	106.5[c]	
Vibrational frequencies (cm^{-1})					
ω_1	3898	3480[e]			3485[e]
ω_2	1005	1084[d]			
ω_3	3655	3609[d]			3624[c]
ω_4	1703	1680[d]			1678[c]
Inversion barrier (cm^{-1})	1959	1783[a]	1792[b]	1867[c]	1885[f]
N–H distance at inversion saddle point (Å)	0.998	0.995[a]	0.994[b]	0.996[c]	
Vibrational frequenices at the saddle point (cm^{-1})					
ω_1	3252	3637[g]			
ω_2	903i	822i[g]			
ω_3	3523	3835[g]			
ω_4	1596	1577[g]			
N–H bond dissociation energy D_e(eV)	4.40	4.70[h]			
V_2					
Energy at minimum-energy geometry (eV)	5.75	5.76[h]			5.72[i]
Equilibrium geometry (Å and deg)					
r_1	1.043	1.048[h]			1.08[i]
θ_1	120	120[h]			120[i]
Saddle point of the N–H dissociation					
Barrier height for N–H dissociation (cm^{-1})	2931	2639[h]			2348[j]
Saddle-point energy (eV)	6.11	6.09[h]			
Saddle-point geometry (Å and deg)					
r_1	1.270	1.302[h]			1.323
r_2	1.070	1.041[h]			1.042
r_3	1.070	1.041[h]			1.042
θ_1	120	114[h]			
θ_2	120	123[h]			
θ_3	120	123[h]			
β	90	90			
Intersection of V_1 and V_2					
Lowest-energy intersection (eV)	4.93				
Geometry of the lowest-energy intersection (Å and deg)					
r_1	2.37				
r_2	1.020				
r_3	1.020				
θ_1	120				
θ_2	120				
θ_3	90				
β	90				

[a]Reference 54.
[b]Reference 55.
[c]Reference 56.
[d]Reference 57.
[e]Reference 58.
[f]Reference 59.
[g]Reference 47.
[h]Reference 9.
[i]Reference 4.
[j]Reference 25.

The key features in the excited adiabatic states that depend strongly on the shape of the U_{22} surface are the excited-state minimum-energy geometry, the conical intersection, and the barrier for photodissociation. Table II shows the MUE in U_{22} as a function of energy. In the low-energy regions ($E<5$ eV) the MUE is 0.09 eV, whereas for geometries with energies below $E<10$ eV the mean unsigned error is 0.19 eV.

TABLE V. Comparison of the adiabatic energies for conical intersection geometries of Ref. 9 with the MC-QDPT results. Distances are in Å, angles are in degrees, and energies are in eV.

	Internal coordinates[a]						Ref. 9		MC-QDPT	
Symmetry	r_1	r_2	r_3	θ_1	θ_2	θ_3	V_1	V_2	V_1	V_2
C_{2v}	1.955	1.021	1.021	110	125	125	5.11	5.11	5.02	5.05
	1.8	1.066	1.066	86	137	137	5.50	5.50	4.93	5.47
	1.6	1.175	1.175	62	149	149	6.95	6.95	6.54	6.90
	1.5	1.265	1.265	52	154	154	7.96	7.96	7.66	8.14
C_s	1.8	1.033	1.033	103	89	168	5.28	5.24	5.11	5.30
	1.6	1.014	1.164	118	73	169	5.77	5.77	5.01	5.76
	1.6	1.014	1.164	138	63	159	6.03	6.03	5.06	6.47

[a]For all points in this table, the final internal coordinate β is $\pi/2$.

The U_{12} coupling is an odd function of $(\beta-\pi/2)$ and changes sign when the system passes through planar geometries. The values of U_{12} range between −2 and +2 eV. Figure 3 shows U_{12} as a function of bond distance and the inversion angle for geometries where one of N–H bonds is stretched. Table III lists the MUE as a function of energy for the fit of U_{12}.

The adiabatic potential-energy surfaces V_1 and V_2 are obtained for a given geometry without any further approximation by diagonalizing Eq. (14), i.e.,

$$V_{1(2)}(\mathbf{Q}) = \tfrac{1}{2}[U_{11}(\mathbf{Q}) + U_{22}(\mathbf{Q})] \mp \tfrac{1}{2}\sqrt{[U_{22}(\mathbf{Q}) - U_{11}(\mathbf{Q})]^2 + 4U_{12}^2(\mathbf{Q})}. \quad (32)$$

Figure 4 shows (a) the smooth crossing between the U_{11} and U_{22} diabatic surfaces and (b) the conical intersection between the ground state V_1 and the first excited state V_2. The plots show how the U_{12} coupling splits the surfaces and gives rise to a conical intersection. A plot of the adiabatic surfaces for a wide range of inversion angle is shown in Fig. 5. Figure 6 is a contour plot of V_2 for a region that includes the excited-state minimum and saddle point for the dissociation.

Having obtained the adiabatic surfaces we can characterize them in terms of their key features. This is done in Table IV, where the results are compared to the best previous[4,9,25,47,54–59] estimates when available. For the ground-state V_1 potential-energy surface the equilibrium N–H distance r_{eq} is 1.010 Å, and the HNH equilibrium angle θ_{eq} is 108.4°. Both these values are in good agreement to the best previous estimates.[54–56] The vibrational frequencies at the ground-state equilibrium geometry are 3898, 1005, 3655, and 1703 cm^{-1} and are in reasonable agreement with the previous theoretical[57] and experimental[58] values. The N–H distance at the inversion saddle point is 0.998 Å, and the inversion barrier height is 1959 cm^{-1}. The vibrational frequencies at the saddle point are listed in Table IV. The N–H bond dissociation energy D_e is 4.40 eV.

The excited-state minimum-energy geometry and the energy at that geometry are listed in Table IV and are in good agreement with previous best estimates.[4,9] The excited-state saddle point along the N–H dissociation coordinate is a C_{2v} geometry the with a barrier height of 2931 cm^{-1}. The values of the internal coordinates at this saddle point are listed in Table IV. Also in Table IV, the geometry and the energy for the lowest-energy conical intersection are listed.

The conical intersections of a molecule occur in at most a $(3N-8)$-dimensional manifold, where N is the number of atoms. For ammonia, $N=4$ and thus the intersection manifold is at most four dimensional. However, U_{12} apparently vanishes only for planar geometries, which form a five-dimensional manifold, because $(2N-3)=5$. However, although U_{12} is zero for all planar geometries, U_{11} does not equal to U_{22} for all planar geometries. This again shows that the conical intersection manifold is at most four dimensional. In particular, it consists of all planar geometries for which

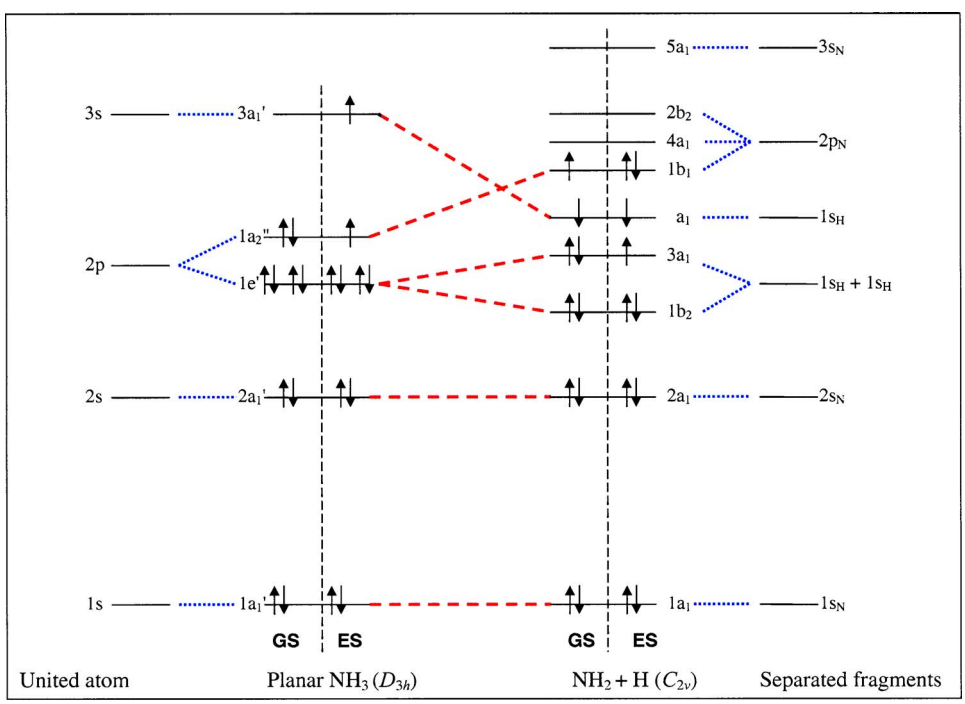

FIG. 7. (Color online) Correlation of orbitals at large and small internuclear distances of ammonia molecule in planar D_{3h} geometry and dissociated NH_2+H fragment in C_{2v} point group for both the ground and the first excited states. At the extreme left are the atomic orbitals of the united atom, and on the extreme right are the orbitals for the separated fragments. The ground-state (GS) and excited-state (ES) electronic configurations are separated by vertical dashed line for both NH_3 and NH_2 molecules. The transformation of orbitals from D_{3h} to C_{2v} is shown by horizontal dashed lines, whereas for that between united atom to NH_3 and NH_2 to separated fragments it is shown by dotted lines. The arrows in the orbitals represent the electrons.

TABLE VI. Dimensionalities.

Space	Dimensions			
	Nonplanar	C_s	C_{2v}	D_{3h}
Full	6	5	3	1
Conical intersection	4	4	2	0[a]

[a]A zero-dimensional seam is a point.

$U_{11}=U_{22}$. The D_{3h} manifold is one dimensional, but $U_{11}=U_{22}$ at only a subset of this manifold. The C_{2v} manifold is three dimensional, and the conical intersection need not be restricted to C_{2v} geometries. In fact, Yarkony[9] showed that the conical intersection manifold is not restricted to the three-dimensional C_{2v} manifold but also includes C_s geometries. In particular, Yarkony found four C_{2v} points and three C_s points on the conical intersection. Since we have analytic representation of the diabatic potentials, setting U_{11} equal to U_{22} for planar geometries gives an analytic representation of the entire conical intersection manifold. We are not restricted to a finite number of points of intersection. Nevertheless the only way to compare to the previous calculations is carry out calculations at Yarkony's seven points of intersection; this is done in Table V. We see that the splitting of our adiabatic potentials at these seven points is 0.03, 0.46, 0.48, 0.54, and 1.41 eV, respectively. Thus we are not in quantitative agreement for the location of the seam. It is not clear which calculation is more reliable. In particular, Yarkony uses a larger active space and more contracted basis functions on nitrogen atom; he also used multireference configuration interaction, which is more complete than multireference perturbation theory. However, and this may be the most important difference, he obtained orbitals by a CASSCF calculation averaged over three states, whereas we averaged over only two, which should be more accurate for the two states under consideration here. Furthermore, we used more contracted functions on each hydrogen atom. Further work will be necessary to understand the quantitative importance of the differences. The question then arises of which additional geometries are contained in the conical intersection manifold.

For ammonia, the presence of a conical intersection and the crossing of a diabatic states can be understood by a group theoretical treatment. In particular, consider a set of geometries at which ammonia is planar, and use the irreducible representations of the D_{3h} point group to label the ground and the first excited electronic states. Figure 7 shows the correlation diagram for the orbitals of NH_3 (in the D_{3h} point group) and those of NH_2+H (in the C_{2v} point group). Along the abscissa is a generalized coordinate representing one (on the right) or three (on the left) N–H internuclear distances, and along ordinate (but not to scale) are the energies of the orbitals. The energies of the united atom with $1s$, $2s$, $2p$, and $3s$ atomic orbitals are shown on the extreme left in Fig. 7, while those for separated NH_2 and H fragments are shown on the extreme right. Next to the united atom, we show the electronic configuration in planar NH_3 with spin-up and spin-down electrons represented by arrows. The ground state (GS) of ammonia is $(1a_1')^2(2a_1')^2(1e')^4(1a_2'')^2$, and the first excited state (ES) is $(1a_1')^2(2a_1')^2(1e')^4(1a_2'')^1(3a_1')^1$. Next to the ex-

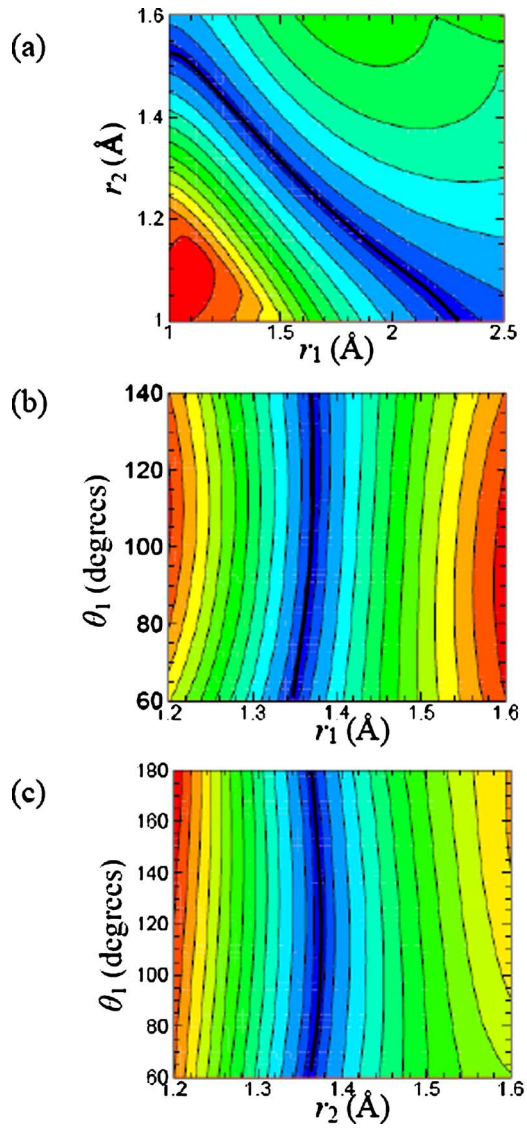

FIG. 9. (Color online) Contour plots of conical intersections of ammonia in C_{2v} geometries. Plot of V_2-V_1 with respect to varying (a) r_1 and r_2, with $r_2=r_3$ and $\theta_1=\theta_2=\theta_3=120°$; (b) r_1 and θ_1, with $r_2=r_3=1.39$ Å and $\theta_2=\theta_3$; (c) r_2 and θ_1, with $r_2=r_3$ for all geometries, $\theta_2=\theta_3$, and $r_1=1.39$ Å. The contour spacing is 0.5 eV for (a), 0.1 eV for (b), and 0.2 eV for (c). In each plot the null contour showing the conical intersection seam is marked by a solid black contour.

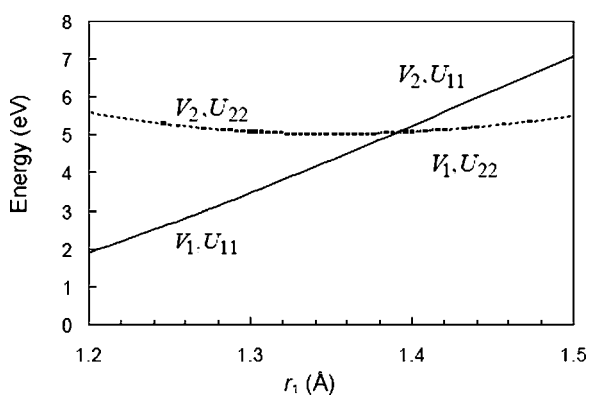

FIG. 8. Cut through the potential-energy surfaces for D_{3h} geometries. For such geometries $V_1=\min(U_{11},U_{22})$ and $V_2=\max(U_{11},U_{22})$. Note that although the results are plotted vs r_1, for D_{3h} geometries, $r_1=r_2=r_3$.

treme right are the molecular-orbital energies corresponding to the orbitals of NH_2+H (C_{2v}). The 1s orbitals of two H atoms in NH_2 give molecular orbitals b_2 and a_1 (in C_{2v}), and the orbital of the separated third H atom has a_1 symmetry. The ground electronic configuration of NH_2 is $(1a_1)^2(2a_1)^2(1b_2)^2(3a_1)^2(1b_1)^1$, and the first excited electronic configuration is $(1a_1)^2(2a_1)^2(1b_2)^2(3a_1)^1(1b_1)^2$, as shown in Fig. 7. The transformation of the irreducible representations from D_{3h} to C_{2v} (shown by dashed lines in Fig. 7) is carried out using the correlation tables of Herzberg.[60] We find that as we transform from the D_{3h} to the C_{2v} point group the highest occupied molecular orbital (HOMO) $(1a_2'')^2$ of ground-state D_{3h} ammonia transforms as $(1b_1)^2$, and the lowest unoccupied molecular orbital (LUMO) $(3a_1')$ of ground-state D_{3h} ammonia transforms as $(3a_1)$. As the N–H distance increases, the relative energy difference between the HOMO $1a_2''$ and the LUMO $3a_1'$ decreases, and at large N–H distances, the $3a_1$ orbital has a lower energy than the b_1 orbital. Since the $1a_2''$ and the $3a_1'$ orbitals are of different symmetry, they can cross each other. Note that at the crossover point, $1a_2''$ and $3a_1'$ are degenerate, and the electronic configuration of the ground $(1a_1')^2(2a_1')^2(1e')^4(1a_2'')^2(3a_1')^0$ and the excited $(1a_1')^2(2a_1')^2(1e')^4(1a_2'')^1(3a_1')^1$ electronic states give the same adiabatic energy. Thus, in an uncorrelated treatment, the crossover point is the location of the conical intersection. Adding correlation energy changes the quantitative location of the conical intersection, but the qualitative nature of the states remains as just described.

The overall symmetry of the electronic states is obtained by carrying out direct product of the irreducible representations of the molecular orbitals. The orbital picture just described is consistent with the earlier observation that the ground electronic state of the NH_2 products ($^2B_1$) correlates diabatically with the first excited ($^1A_2''$) state of NH_3, while the first excited state of NH_2 products ($^2A_1$) correlates diabatically with the ground state ($^1A_1$) of ammonia. Note that here we have used the standard convention to use lowercase letters to represent the symmetry of the orbitals and upper case letters to represent the overall symmetry of the electronic states.

Although the considerations involving the orbitals of Fig. 7 provide a qualitative understanding of the intersection, our surface fits allow a more complete discussion of the multidimensional shape of the four-dimensional (4D) conical intersection seam. Table VI summarizes the relevant dimensionalities. Since all planar geometries have $U_{12}=0$, the dimensionality of the seam is one lower than the full dimensionality for planar geometries, as illustrated in the last three columns of Table VI. We will start in the last column (D_{3h}) and then successively lower the symmetry to C_{2v} and C_s. Figure 8 allows us to identify the conical intersection within the one-dimensional D_{3h} manifold and it shows a conical intersection at the point where the N–H distance is equal to 1.390 Å. Starting from this D_{3h} conical intersection geometry we then systematically lower the symmetry to C_{2v} geometries so as to explore the three-dimensional C_{2v} manifold. We keep three internal coordinates fixed at the D_{3h} conical intersection geometry and vary two coordinates simultaneously, and the intersection shows up as the null contour in a contour map of V_2-V_1 versus the two varying coordinates. Figures 9(a)–9(c) show such contour plots of conical intersections seams in the C_{2v} manifold. We further lower the symmetry from C_{2v} to C_s to explore the four-dimensional C_s seam. This is done by choosing a C_{2v} geometry from the conical intersection seam in Fig. 9 and varying any one of the internal coordinates with the remaining four fixed. The conical intersection then shows up as a point as shown in Figs. 10(a)–10(f). Additional cuts of C_s geometries where the conical intersection shows up as a point are shown in Fig. 11. With analytic fits to the diabats, it is relatively straight forward to make plots like Figs. 8–11 that completely map out the conical intersection scheme. These figures show that it is now possible to fully map out a conical intersection scheme rather than simply searching for isolated high-symmetry and low-symmetry points on the seam.

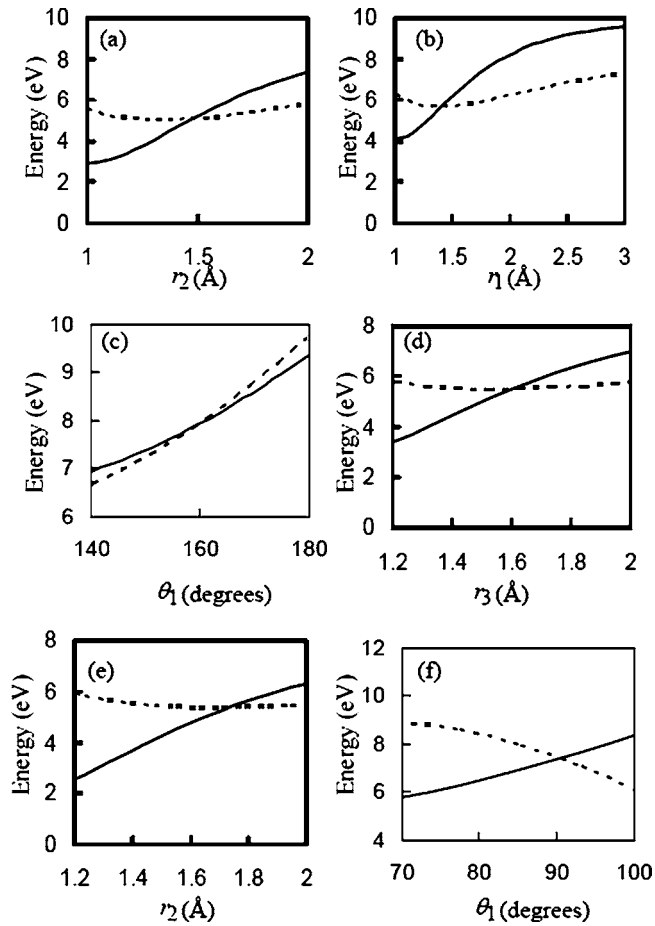

FIG. 10. Cuts through the diabatic potential-energy surfaces of ammonia, U_{11} (solid) and U_{22} (dashed), for C_s geometries. The plots attempt to map out the conical intersections in C_s geometries by moving along one internal coordinates starting from a C_{2v} geometry. The fixed internal coordinates are (a) $r_1=1.2$ Å, $r_3=1.5$ Å, and $\theta_1=\theta_2=\theta_3=120°$; (b) $r_2=r_3=1.39$ Å, $\theta_1=120°$, $\theta_2=150°$, and $\theta_3=90°$; (c) $r_1=1.5$ Å, $r_2=r_3=1.39$ Å, and $\theta_2=155°$; (d) $r_1=1.2$ Å, $r_2=1.39$ Å, $\theta_1=90°$, and $\theta_2=\theta_3=135°$; (e) $r_1=1.39$ Å, $r_3=1.05$ Å, $\theta_1=140°$, and $\theta_2=110°$; (f) $r_1=1.36$ Å, $r_2=r_3=1.0$ Å, and $\theta_2=120°$. For planar geometries, the adiabats are $V_1=\min(U_{11},U_{22})$ and $V_2=\max(U_{11},U_{22})$.

V. CONCLUSIONS

In this paper we have used the fourfold-way diabatization scheme to obtain diabatic potential-energy surfaces and

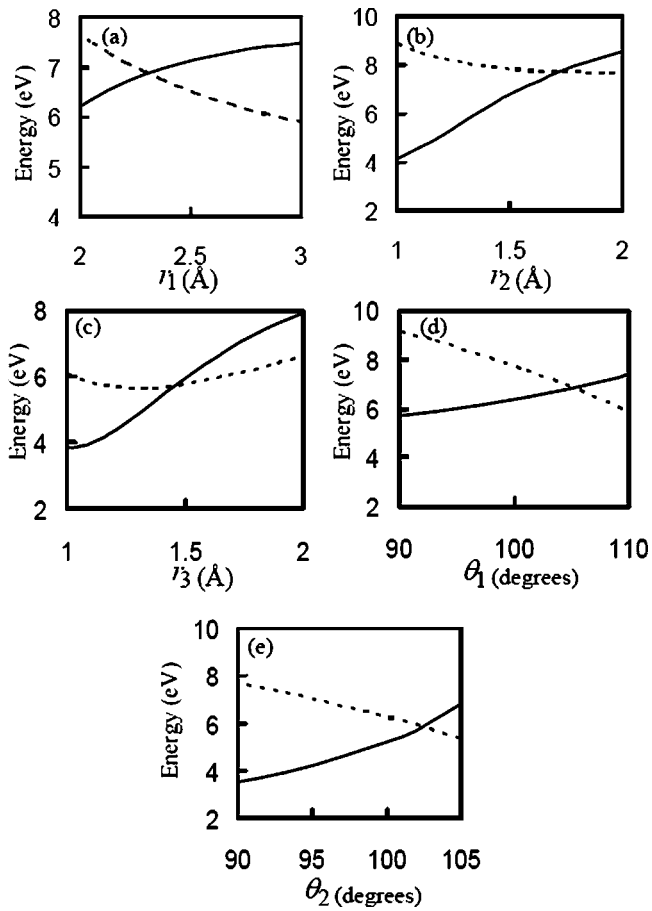

FIG. 11. Cuts through the diabatic potential-energy surfaces of ammonia, U_{11} (solid) and U_{22} (dashed), for C_s geometries along one internal coordinate with the rest of the coordinates fixed in planar geometry. The fixed internal coordinates are (a) $r_2=r_3=1.08$ Å, $\theta_1=103°$, and $\theta_2=89°$; (b) $r_1=1.5$ Å, $r_3=1.4$ Å, $\theta_1=103°$, and $\theta_2=89°$; (c) $r_1=1.65$ Å, $r_2=1.1$ Å, $\theta_1=102°$; and $\theta_2=150°$; (d) $r_1=1.45$ Å, $r_2=1.25$ Å, $r_3=1.17$ Å, and $\theta_2=120°$; (e) $r_1=1.5$ Å, $r_2=1.1$ Å, $r_3=1.2$ Å, and $\theta_1=127°$. For planar geometries, the adiabats are $V_1=\min(U_{11},U_{22})$ and $V_2=\max(U_{11},U_{22})$.

couplings for ammonia. The method performed quite satisfactorily and yields globally smooth diabatic potentials. We then fit analytic global functions incorporating the correct permutation symmetry. This method allows us to avoid the problem of fitting surfaces in the adiabatic representation where conical intersections and avoided crossings are not smooth. The direct diabatic calculations not only make fitting the potential-energy surface more convenient and provide an unprecedented analytic representation of a four-dimensional intersection seam, they also provide a scalar, smooth, and a singularity-free representation of the potential-energy surfaces and couplings for dynamical calculations.

ACKNOWLEDGMENTS

The authors thank Hisao Nakamura for helpful discussions. This work was supported in part by the National Science Foundation under Grant No. CHE03-49122 and by the Office of Naval Research under Grant No. ONR-N00014-01-1-0235.

[1] L. D. Ziegler, J. Chem. Phys. **82**, 664 (1985).
[2] M. N. R. Ashfold, C. L. Bennett, and R. N. Dixon, Faraday Discuss. Chem. Soc. **82**, 163 (1986).
[3] P. Rosmus, P. Botschwina, H.-J. Werner, V. Vaida, P. C. Engelking, and M. I. McCarthy, J. Chem. Phys. **86**, 6677 (1987).
[4] M. I. McCarthy, P. Rosmus, H.-J. Werner, P. Botschwina, and V. Vaida, J. Chem. Phys. **86**, 6693 (1987).
[5] R. N. Dixon, Mol. Phys. **68**, 263 (1989).
[6] S. L. Tang, E. H. Abramson, and D. G. Imre, J. Phys. Chem. **95**, 4969 (1991).
[7] S. L. Tang and D. G. Imre, J. Phys. Chem. **95**, 4976 (1991).
[8] R. N. Dixon, Mol. Phys. **88**, 949 (1996).
[9] D. R. Yarkony, J. Chem. Phys. **121**, 628 (2004).
[10] V. Vaida, M. I. McCarthy, P. C. Engelking, P. Rosmus, H.-J. Werner, and P. Botschwina, J. Chem. Phys. **86**, 6669 (1987).
[11] R. N. Dixon, Chem. Phys. Lett. **147**, 377 (1988).
[12] J. Biesner, L. Schnieder, G. Ahlers, X. Xie, K. H. Welge, M. N. R. Ashfold, and R. N. Dixon, J. Chem. Phys. **88**, 3607 (1988).
[13] J. Biesner, L. Schnieder, G. Ahlers, X. Xie, K. H. Welge, M. N. R. Ashfold, and R. N. Dixon, J. Chem. Phys. **91**, 2901 (1989).
[14] E. L. Woodbridge, M. N. R. Ashfold, and S. R. Leone, J. Chem. Phys. **94**, 4195 (1991).
[15] M. N. R. Ashfold, C. M. Western, J. W. Hudgens, and R. D. Johnson, Chem. Phys. Lett. **260**, 27 (1996).
[16] D. H. Mordaunt, M. N. R. Ashfold, and R. N. Dixon, J. Chem. Phys. **104**, 6460 (1996).
[17] D. H. Mordaunt, R. N. Dixon, and M. N. R. Ashfold, J. Chem. Phys. **104**, 6472 (1996).
[18] R. N. Dixon and T. W. R. Hancock, J. Phys. Chem. A **101**, 7567 (1997).
[19] M. N. R. Ashfold, R. N. Dixon, M. Kono, D. H. Mordaunt, and C. L. Reed, Philos. Trans. R. Soc. London, Ser. A **355**, 1659 (1997).
[20] I. Kleiner, L. R. Brown, G. Tarrago, Q. L. Kou, N. Picque, G. Guelachvili, V. Dana, and J. Y. Mandin, J. Mol. Spectrosc. **193**, 46 (1999).
[21] R. A. Loomis, J. P. Reid, and S. R. Leone, J. Chem. Phys. **112**, 658 (2000).
[22] J. P. Reid, R. A. Loomis, and S. R. Leone, J. Chem. Phys. **112**, 3181 (2000).
[23] J. P. Reid, R. A. Loomis, and S. R. Leone, Chem. Phys. Lett. **324**, 240 (2000).
[24] J. P. Reid, R. A. Loomis, and S. R. Leone, J. Phys. Chem. A **104**, 10139 (2000).
[25] A. Bach, M. J. Hutchison, R. J. Holiday, and F. F. Crim, J. Chem. Phys. **116**, 4955 (2002).
[26] A. Bach, M. J. Hutchison, R. J. Holiday, and F. F. Crim, J. Chem. Phys. **116**, 9315 (2002).
[27] A. Bach, M. J. Hutchison, R. J. Holiday, and F. F. Crim, J. Phys. Chem. A **107**, 10490 (2003).
[28] A. Bach, M. J. Hutchison, R. J. Holiday, and F. F. Crim, J. Chem. Phys. **118**, 7144 (2003).
[29] H. Akagi, K. Yokoyama, and A. Yokoyama, J. Chem. Phys. **118**, 3600 (2003).
[30] H. Akagi, K. Yokoyama, and A. Yokoyama, J. Chem. Phys. **120**, 4696 (2004).
[31] C. A. Mead, J. Chem. Phys. **78**, 807 (1983).
[32] A. W. Jasper, B. K. Kendrick, C. A. Mead, and D. G. Truhlar, Adv. Ser. Phys. Chem. **14**, 329 (2004).
[33] G. J. Achity and K. Ruedenberg, Theor. Chem. Acc. **97**, 47 (1997), and references cited therein.
[34] H. Nakamura and D. G. Truhlar, J. Chem. Phys. **115**, 10353 (2001), and references cited therein.
[35] H. Nakamura and D. G. Truhlar, J. Chem. Phys. **117**, 5576 (2002).
[36] H. Nakamura and D. G. Truhlar, J. Chem. Phys. **118**, 6816 (2003).
[37] C. A. Mead and D. G. Truhlar, J. Chem. Phys. **77**, 6090 (1982).
[38] B. K. Kendrick, C. A. Mead, and D. G. Truhlar, Chem. Phys. **277**, 31 (2002).
[39] H. Nakano, J. Chem. Phys. **99**, 7983 (1993).
[40] H. Nakano, T. Nakajima, T. Tsuneda, and H. Hirao, THEOCHEM **573**, 91 (2001).
[41] B. O. Roos, Adv. Chem. Phys. **69**, 399 (1987).
[42] R. Krishnan, J. S. Binkley, R. Seeger, and J. A. Pople, J. Chem. Phys. **72**, 650 (1980).
[43] M. J. Frisch, J. A. Pople, and J. S. Binkley, J. Chem. Phys. **80**, 3265 (1984).
[44] H. Nakamura, J. D. Xidos, J. D. Thompson, J. Li, T. Zhu, B. J. Lynch, Y.

Volobuev, D. A. Liotard, C. J. Cramer, and D. G. Truhlar, HONDOPLUS, v.4.6, University of Minnesota, Minneapolis, 2004, based on HONDO, v.99.6.
[45] M. Dupuis, A. Marquez, and E. R. Davidson, HONDO, v.99.6, University of Minnesota, Minneapolis, 1999, based on HONDO, v.95.3; M. Dupuis, A. Marquez, and E. R. Davidson, Quantum Chemistry Program Exchange (QCPE), Indiana University, Bloomington, IN 47405.
[46] N. C. Handy, S. Carter, and S. M. Cowell, Mol. Phys. **96**, 477 (1999).
[47] C. Léonard, N. C. Handy, S. Carter, and J. M. Bowman, Spectrochim. Acta, Part A **58**, 825 (2002).
[48] X. Huang, S. Carter, and J. M. Bowman, J. Phys. Chem. B **106**, 8182 (2002).
[49] C. Léonard, S. Carter, and N. C. Handy, Chem. Phys. Lett. **370**, 360 (2003).
[50] D. E. Rutherford, *Substitutional Analysis* (Hafner, New York, 1968).
[51] See EPAPS Document No. E-JCPSA6-124-006607 for a brief description of permutation matrices, comments on the indices used in the fits, and list of nonlinear parameters and coefficients used in the fitting of the diabatic potential-energy surfaces. This document can be reached via a direct link in the online article's HTML reference section or via the EPAPS homepage (http://www.aip.org/pubservs/epaps.html).
[52] R. J. Duchovic, Y. L. Volobuev, G. C. Lynch, D. G. Truhlar, T. C. Allison, A. F. Wagner, B. C. Garrett, and J. C. Corchado, Comput. Phys. Commun. **144**, 169 (2002); **156**, 319(E) (2004).
[53] R. J. Duchovic, Y. L. Volobuev, G. C. Lynch, A. W. Jasper, D. G. Truhlar, T. C. Allison, A. F. Wagner, B. C. Garrett, J. Espinosa-García, and J. C. Corchado, POTLIB-online, http://comp.chem.umn.edu/potlib
[54] H. Lin, W. Thiel, S. N. Yurchenko, M. Carvajal, and P. Jensen, J. Chem. Phys. **117**, 11265 (2003).
[55] T. Rajamäki, A. Miani, and L. Halonen, J. Chem. Phys. **118**, 10929 (2003).
[56] J. Pesonen, A. Miani, and L. Halonen, J. Chem. Phys. **115**, 1243 (2001).
[57] J. M. L. Martin, T. J. Lee, and P. R. Taylor, J. Chem. Phys. **97**, 8361 (1992).
[58] S. L. Coy and K. K. Lehmann, Spectrochim. Acta, Part A **45**, 47 (1989).
[59] V. Špirko and W. P. Kraemer, J. Mol. Spectrosc. **133**, 331 (1989).
[60] G. Herzberg, *Molecular Spectra and Molecular Structure of Polyatomic Molecules* (Van Nostrand, New York, 1966), p. 577.